



Published in final edited form as:

*J Mater Chem B Mater Biol Med.* 2016 April 14; 4(14): 2428–2434. doi:10.1039/C5TB02172C.

## Biodistribution and fate of core-labeled $^{125}\text{I}$ polymeric nanocarriers prepared by Flash NanoPrecipitation (FNP)

Christina Tang<sup>1,2</sup>, Jasmine Edelstein<sup>1,2</sup>, John L Mikitsh<sup>3</sup>, Edward Xiao<sup>1,3</sup>, Aaron H Hemphill II<sup>4</sup>, Robert Pagels<sup>1</sup>, Ann-Marie Chacko<sup>3,4,\*</sup>, and Robert Prud'homme<sup>1</sup>

<sup>1</sup> Department of Chemical and Biological Engineering, Princeton University, Princeton, NJ United States

<sup>2</sup> Department of Chemical and Life Science Engineering, Virginia Commonwealth University, Richmond, VA, United States

<sup>3</sup> Department of Radiology, Division of Nuclear Medicine and Clinical Molecular Imaging

<sup>4</sup> Department of Radiation Oncology

### Abstract

Non-invasive medical imaging techniques such as positron emission tomography (PET) imaging are powerful platforms to track the fate of radiolabeled materials for diagnostic or drug delivery applications. Polymer-based nanocarriers tagged with non-standard PET radionuclides with relatively long half-lives (e.g.  $^{64}\text{Cu}$ :  $t_{1/2} = 12.7$  h,  $^{76}\text{Br}$ :  $t_{1/2} = 16.2$ h,  $^{89}\text{Zr}$ :  $t_{1/2} = 3.3$  d,  $^{124}\text{I}$ :  $t_{1/2} = 4.2$  d) may greatly expand applications of nanomedicines in molecular imaging and therapy. However, radiolabeling strategies that ensure stable *in vivo* association of the radiolabel with the nanocarrier remain a significant challenge. In this study, we covalently attach radioiodine to the core of pre-fabricated nanocarriers. First, we encapsulated polyvinyl phenol within a poly(ethylene glycol) coating using Flash NanoPrecipitation (FNP) to produce stable 75 nm and 120 nm nanocarriers. Following FNP, we radiolabeled the encapsulated polyvinyl phenol with  $^{125}\text{I}$  via electrophilic aromatic substitution in high radiochemical yields (> 90%). Biodistribution studies reveal low radioactivity in the thyroid, indicating minimal leaching of the radiolabel *in vivo*. Further, PEGylated [ $^{125}\text{I}$ ]PVPh nanocarriers exhibited relatively long circulation half-lives ( $t_{1/2\alpha} = 2.9$  h,  $t_{1/2\beta} = 34.9$  h) and gradual reticuloendothelial clearance, with 31% of injected dose in blood retained at 24 h post-injection.

### Keywords

Flash NanoPrecipitation (FNP); nanocarrier; radioiodine; nanoparticle; biodistribution; self-assembly

\*Current address is Duke-NUS Graduate Medical School, Singapore, 169857

## 1. Introduction

Molecular imaging with radiolabeled compounds using positron emission tomography (PET) enables non-invasive visualization and quantification of ligand biodistribution and tissue-specific pharmacokinetics with high sensitivity ( $<M^{-10}$ ).<sup>1,2</sup> Conventional radionuclides have short half-lives (e.g.  $^{15}O$ :  $t_{1/2} = 2$  min,  $^{13}N$ :  $t_{1/2} = 10$  min,  $^{11}C$ :  $t_{1/2} = 20.4$  min,  $^{18}F$ :  $t_{1/2} = 109.8$  min), limiting the time frame for radiosynthesis and *in vivo* imaging.<sup>3-5</sup> Nanocarrier applications for delivery by EPR (enhanced permeation and retention) or targeting require longer circulation times; and therefore require non-standard radionuclides with longer half-lives (e.g.  $^{64}Cu$ :  $t_{1/2} = 12.7$  h,  $^{76}Br$ :  $t_{1/2} = 16.2$  h,  $^{89}Zr$ :  $t_{1/2} = 3.2$  d  $^{124}I$ :  $t_{1/2} = 4.2$  d).<sup>6,7</sup>

There have been two approaches for PET labeling nanocarriers. Most commonly, chelators have been introduced on the surfaces of the nanocarriers which are subsequently complexed with the PET cation.<sup>8,9</sup> However, attachment of chelates and radionuclides to the surface of nanoprobe can add surface charge, triggering adsorption of plasma proteins and a RES response.<sup>3, 10-13</sup> Further, early detachment of these radionuclides from their nanoprobe anchors *in vivo* confounds accuracy of probe distribution results.<sup>14-26</sup> Radionuclide detachment can occur due to kinetically unstable radiometal chelate systems or metabolic degradation of the nanocarrier-radiolabel linkage.<sup>8, 27, 28</sup> The second approach is to synthesize the nanocarrier core as a metal oxide or sulfide of the PET cation. For example, Zhou *et al.* generated chelator-free PEGylated [ $^{64}Cu$ ]CuS nanocarriers, but the size was limited to 30 nm.<sup>29</sup> The time required for the synthesis of these radioactive cores sacrifices radioactive activity; the complexity of synthesis, and the difficulty in subsequent passivation of the metal particle with a biocompatible coating, make this approach problematic. Biocompatible coatings, such as by poly(ethylene glycol) (PEG), is required to delay reticuloendothelial (RES) clearance and improve circulation times.<sup>13,14,30,31</sup>

The particles and process we describe here are the first to address all of the limitations currently encountered in PET active nanocarriers. Ideally, nanocarriers and processes to produce them should have the following characteristics: (1) they can be produced over a range of sizes, (2) the radionuclides are covalently bound to the carrier by a straightforward and rapid process, (3) the core, rather than just the surface, is labeled to avoid addition of surface charge and increase radionuclide loading (surface attachment suffers from the surface to volume limitation), and finally, (4) the carrier requires a dense PEG coating to enable long circulation, and possibly provide a platform for targeting. Thus, our goal was to develop a strategy to radiolabel the core of pre-fabricated PEGylated nanocarriers. We focused on radiolabeling nanocarriers with the low-energy gamma emitter  $^{125}I$  ( $t_{1/2} = 60$  days) to facilitate optimization of radiolabeling and assess *in vitro* and *in vivo* properties.<sup>7</sup> The same chemistry can be used to radiolabel nanocarriers with higher energy radioiodines, including  $^{124}I$  or  $^{123}I$  for PET or SPECT imaging, respectively. Since radioiodination of phenols has been well studied, we encapsulated poly-4-vinyl phenol (PVPh) within PEGylated nanocarriers to provide a stable nanocarrier core and site for radioiodine conjugation.

In Flash NanoPrecipitation (FNP) (Figure 1), hydrophobic core material (e.g. PVPh) and amphiphilic block copolymer (e.g. PEG-*b*-polystyrene (PS)) are dissolved in an organic phase and rapidly mixed with a miscible aqueous anti-solvent. Rapid mixing causes nucleation and growth of the precipitating core material. The hydrophobic segment of the block copolymer adsorbs to the hydrophobic precipitate, arresting nanocarrier growth as the hydrophilic PEG block sterically stabilizes the colloidal nanocarriers.<sup>32,33</sup> As a process of kinetic assembly, FNP provides control over nanocarrier size from 40 nm to 400 nm with narrow polydispersity.<sup>34,35</sup> Following FNP, we performed <sup>127</sup>I- or <sup>125</sup>I-driven iodination reaction on the nanocarrier PVPh core to examine the accessibility of the encapsulated polyvinyl phenol for electrophilic aromatic substitution. The *in vivo* fate and biodistribution of the nanocarriers radiolabeled with <sup>125</sup>I were studied with nanocarriers.

## 2. Experimental

### Materials

ACS grade sodium iodide, D- $\alpha$ -tocopherol, and chloramine-T trihydrate were purchased from Sigma Aldrich. HPLC grade tetrahydrofuran (THF) was obtained from Fisher Scientific. Phosphate buffered saline without Ca<sup>2+</sup> and Mg<sup>2+</sup> was obtained from Lonza. Block copolymer, PEG<sub>5000</sub>-*block*-PS<sub>1600</sub>, was from Polymer Source (Dorval, QC, CAN) and PVPh<sub>1500-7000</sub> was from Polysciences, Inc. (Warrington, PA). All materials were used as received. Water (MQ) was purified by 0.2  $\mu$ m filtration and four-stage deionization to a resistivity of 17 M $\Omega$  or greater (NANOpure Diamond, Barnstead International, Dubuque, IA).

### Nanocarrier Synthesis and Characterization

FNP was performed using a hand-operated confined impinging jet mixer with dilution as previously described.<sup>36</sup> The amphiphilic stabilizer PEG-*b*-PS and core material(s) PVPh and D- $\alpha$ -tocopherol were dissolved in THF (40 mg/mL). The ratio of PVPh and D- $\alpha$ -tocopherol was varied to tune the size of the nanoparticles. The organic mixture (typically 1 mL) was rapidly mixed with an equal volume of NANOpure water in a manually operated confined impinging jet mixer (mixing Reynolds number of  $\sim$ 1300)<sup>37</sup> and collected into a stirred water reservoir. The final volume was typically 10 mL containing 10 vol.% organic solvent. After FNP, organic solvent was removed from the suspensions via dialysis using 6-8 kDa MWCO dialysis tubing against 1 L of NANOpure water at room temperature, which was refreshed four times over 24 h. Nanocarriers were concentrated to 10 mg/mL using Amicon® Ultra 3 kDa MWCO centrifugal filters in a centrifuge.

The hydrodynamic diameter and size distribution (PDI) of nanocarriers were measured with a ZetaSizer Nano Dynamic Light Scattering (DLS) device (Malvern Instruments, Worcestershire, UK). Measurements were done in triplicate at a wavelength of 633 nm and a scattering angle of 173°. Nanocarriers were diluted in NANOpure water at a 1:10 ratio so they were translucent. Samples for TEM were prepared by placing 5  $\mu$ L of the nanocarrier dispersion on an Ultrathin Carbon Film on a Holey Carbon Support film on 400 mesh copper grid (Ted Pella, Inc., Redding, CA) and drying under ambient conditions. The

samples were imaged using a Philips CM100 TEM (Eindhoven, The Netherlands) operated at an accelerating voltage of 100 kV.

### Nanocarrier Iodination

PEGylated PVPh nanocarriers (4 mg/mL in deionized water, 100% PVPh core) were iodinated via aromatic electrophilic substitution using a previously reported method<sup>38</sup> to determine if the phenols in the core of the nanocarrier were accessible for iodination. Briefly, sodium iodide (1 eq.) was added to nanocarriers and cooled on ice. Sodium hypochlorite (1 eq.) was added dropwise, every 10-15 sec over 10 min. After 2 h at 0° C, the reaction was quenched by the addition of excess sodium metabisulfite and neutralized using HCl. Following iodination, nanocarrier size was measured by DLS. The reaction mixture was dialyzed against water for 65 h to remove excess sodium iodide, sodium hypochlorite, and PBS salts, and then freeze-dried. Nanocarrier shell components were then redissolved in deuterated DMSO and analyzed using <sup>13</sup>C-NMR on a Bruker Avance-III 500 MHz device (Bruker Biosciences, Inc. Billerica, MA).

### Nanocarrier Radioiodination and Radiolabel Stability

PEGylated PVPh nanocarriers were radiolabeled with [<sup>125</sup>I]NaI (Perkin Elmer, Boston, MA) using a shorter, alternative method. The nanocarriers (200 μL, 10 mg/mL in deionized water) were combined with chloramine-T oxidant solution (2 μL, 17.6 mM in PBS) and [<sup>125</sup>I]NaI (approximately 250 μCi in 2 μL PBS) for 30 min with stirring. Unreacted free radioiodine was removed by using a 10 kDa MWCO Amicon ultracentrifuge filter device (Millipore Inc. Bellerica, MA, USA) at 16,400 g for 15 min. The sample was washed with 300 μL PBS twice, and the purified radiolabeled nanocarriers were recovered by spin inversion. The radiochemical yield and radiochemical purity was assessed by digital autoradiography (DAR) (FLA-7000, FujiFilm Phosphorimager, Tokyo, Japan) of radioTLC SiO<sub>2</sub> silica gel plates. TLC plates were run in 1:1 10% ammonium acetate/methanol and exposed for approximately 1.5 h to the phosphor plate (BAS 2000, Fujifilm) before imaging. Under these conditions, the nanocarrier remains at the origin whereas free radioiodine travels near the solvent front (Supporting Information).

To examine nanocarrier-associated radiolabel stability, triplicate samples of nanocarriers (5 μL, 215 uCi) were added to 100 μL PBS or 100 μL human serum, and incubated with mixing at 37 °C for 0 min, 5 min, 15 min, 30 min, 1 h, 2 h, 4 h, 6 h, 12 h, 24 h, and 48 h. A 1 μL sample was withdrawn at the indicated time point and then spotted for radio-TLC under the TLC conditions listed previously.

### In Vivo Fate and Biodistribution

All animal studies were carried out in accordance with the Guide for the Care and Use of Laboratory Animals as adopted by the US National Institutes of Health and approved by the University of Pennsylvania IACUC. Naive C57BL/6 mice (18-22 g) were anesthetized and nanocarriers (150 μL, 5 mg/kg, 0.1 μCi/μg) injected intravenously via the jugular vein (n = 3 per time point).

Blood samples (approximately 50  $\mu$ L each) were collected via retro-orbital bleeding from anesthetized mice at 2 min, 10 min, 30 min, 1 h, 6 h, and 48 h post-injection. Each sample was weighed, and then radioactivity was measured using a gamma counter (Wizard 2470 Perkin Elmer). Sample-associated radioactivity was measured and radioactivity levels were normalized to the amount of nano-particle bound radioactivity in the injected dose to obtain a fraction of the injected dose in the tissue of interest. Results are reported as either percent of injected dose per gram of tissue (% ID/g) or percent of injected dose per whole organ (% ID) where blood accounts for 7% of mouse body weight.<sup>14,39</sup> Nanoparticle concentration in blood as a function of time post-injection was fit to a bi-exponential decay curve for a standard two compartment pharmacokinetic model. The  $\alpha$ -, and  $\beta$ - half-lives were extrapolated to describing the blood distribution and clearance phase, respectively, using Prism 5.0 (GraphPad) software.

Based on the blood clearance, mice were euthanized at 5 min, 4 h, 10 h, 24 h, and 96 h post-injection and selected organs were harvested and weighed. The liver, spleen, kidney and thyroid were monitored to provide insight into *in vivo* particle stability over 96 hours. Sample-associated radioactivity was measured and radioactivity levels were normalized by the method described above. Results are reported as either percent of injected dose per gram of tissue (% ID/g) or percent of injected dose per whole organ (% ID), where bone accounts for 14% of mouse body weight, respectively.<sup>14,39</sup> All data are expressed as mean  $\pm$  standard deviation.

### 3. Results and Discussion

#### Nanocarrier Synthesis and Characterization

PEGylated PVPh nanocarriers were produced using Flash NanoPrecipitation (FNP). PVPh was dissolved with the amphiphilic block copolymer PEG-*b*-PS in THF, and then rapidly mixing with deionized water (an antisolvent for PVPh). The PEG-*b*-PS self-assembled via hydrophobic interactions between the PS block and PVPh precipitates, while the PEG block sterically stabilizes the nanocarriers. As a process of kinetic assembly, FNP provides control over nanocarrier size – a property that influences *in vivo* performance. According to the literature, nanocarriers larger than 100 nm are easily sequestered in the sinusoids of the spleen and fenestra of the liver, whereas nanocarriers smaller than 20 nm are rapidly filtered by the kidney.<sup>3, 40-44</sup> To create nanocarriers that avoid rapid clearance by these mechanisms, our goal was to produce nanocarriers between 20 and 100 nm.

A representative TEM micrograph of PEGylated PVPh nanocarriers is shown in Figure 2a. The PVPh core of the spherical nanocarriers is evident in the TEM image. Nanocarriers appear smaller than the hydrodynamic radius measured with DLS because the PEG layer is not sufficiently electron dense to be visible with TEM. The PEG layer adds approximately 20 nm to the hydrodynamic diameter.<sup>32</sup> The resulting PVPh-loaded nanocarriers were  $120 \pm 8$  nm with a PDI of  $0.228 \pm 0.008$ .

To reduce the size of the resulting nanocarriers, we co-precipitated the PVPh with D- $\alpha$ -tocopherol (Vitamin E). D- $\alpha$ -tocopherol acts as nucleating agent to seed particle growth via heterogeneous nucleation. Specifically, it lowers the activation energy for particle growth,

induces nucleation, and controls the number of nuclei.<sup>45</sup> Nanocarriers containing a 75:25 wt:wt D- $\alpha$ -tocopherol:PVPPh core were 110 nm with a PDI of  $0.151 \pm 0.009$  (Figure 2b).

### Nanocarrier Iodination

Proteins and peptides containing tyrosine can be radiolabeled via electrophilic aromatic substitution of the phenol moiety. Initially, we use well-established iodination chemistry, using sodium iodide with sodium hypochlorite as the oxidant, to radioiodinate the PVPPh core of the PEGylated nanocarriers.

Our preliminary goal was to establish that the encapsulated PVPPh could be iodinated via electrophilic aromatic substitution. Since the iodination procedure has been reported at a range of pH values,<sup>46,47</sup> we verified that the phenol-containing nanocarriers were stable under potential reaction conditions. The nanocarrier dispersions were stable for at least 4 weeks in deionized water. Variable pH, from 3 to 10, did not significantly affect nanocarrier size. At pH 12, the ionization of phenol destabilizes the nanocarriers (Supporting Information). Nanocarrier size was not significantly affected by the iodination reaction under the specified conditions (Supporting Information).

Following the iodination reaction and purification, we verified that the PVPPh core was radiolabeled in the *ortho* position. <sup>13</sup>C NMR spectroscopy reveals that iodination causes an upfield shift of the carbon signal *ortho* to the phenol from 115 to 84 ppm.<sup>48</sup> Di-iodination of polyvinyl phenol core is evident from the downfield shift of the *ortho* <sup>13</sup>C-I signal to 87 ppm (Figure 3). Using one equivalent of non-radioactive <sup>127</sup>I, 55% of the phenols were iodinated and 54% of the iodinated phenols were di-iodinated. This demonstrated that the iodination reaction reacts in the core of the nanocarrier, and not just on the surface. Furthermore, in higher magnification TEM images the contrast in the iodinated particles appeared uniform (ie uniformly dark from the higher contrast iodine) rather than the iodine being just in a shell on the surface. In separate experiments, no iodine-addition to PEG-*b*-PS under the same non-radioactive iodination conditions were observed by <sup>13</sup>C NMR.

### Nanocarrier Radioiodination and Radiolabel Stability

Using a shorter, alternative procedure, we radiolabeled the PEGylated PVPPh nanocarriers with gamma emitting <sup>125</sup>I, as [<sup>125</sup>I]NaI, being the limiting reagent. The nanocarriers were combined with an oxidant, chloramine-T in PBS and [<sup>125</sup>I]NaI for 30 min with stirring. Following the reaction the nanocarriers were separated from unreacted free radioiodine by ultracentrifugation for 15 minutes (10 kDa MWCO Amicon ultracentrifuge filter device). The sample was washed with 300  $\mu$ L PBS twice, and the purified radiolabeled nanocarriers were recovered by spin inversion. The total procedure time was 80-90 minutes comparable to previously reported radiolabeling experiments.<sup>14,17,49</sup>

Given the results from non-radioactive nanocarrier labeling, our data suggest that radioiodine would be introduced *ortho* to the hydroxyl group of phenol.<sup>14, 50</sup> Under the same conditions as the radioiodination, no iodination of the PEG-*b*-PS was observed as confirmed by <sup>13</sup>C NMR. Post-radioiodination, particles were  $\sim$ 110 nm by DLS compared to  $79 \pm 3$  nm (PDI  $0.151 \pm 0.009$ ). The increase in particle size during radioiodination which was not observed in the initial iodination experiments is likely due to the difference in reaction

conditions. In the initial iodination experiments, the sodium hypochlorite oxidant and iodine was added in excess to the particles and then the nanocarriers were isolated by protracted dialysis. In contrast, in the radioiodination the  $^{125}\text{I}$  is the limiting reagent with Chloramine-T oxidant added in excess. This likely affects particle size.

Radioiodination occurred at high radiochemical yields (>90%) with high radiochemical purity (> 99%). We achieved specific activities of 0.1  $\mu\text{Ci}/\mu\text{g}$  nanocarrier, which is sufficient for biodistribution studies. Only a small fraction (0.01-0.05%) of phenols needed to be radioiodinated because of the large concentration of phenols encapsulated in the nanocarrier core. However, nanocarriers with significantly higher specific activity can be easily synthesized via addition of more radioiodine, which was the stoichiometrically limiting reagent in this synthesis. This offers an advantage compared to chelation which often only enables attachment of tens of radionuclides per particle<sup>51</sup> and will enable acquisition of high-quality images because nanoprobe will have a high signal to noise ratio at lower mass dosages.<sup>52</sup>

Radiochemical stability of radiolabeled nanocarriers *in vitro* was evaluated up to 48 h in PBS and human serum. No free radioiodine was detected with TLC, indicating minimal radiolabel leaching over 48 h (Supporting Information). This initial characterization indicates these nanocarriers are sufficiently stable for *in vivo* fate studies. Separate analysis of particle stability *in vivo* is discussed below.

### In Vivo Fate and Biodistribution

To determine the appropriate time points to evaluate biodistribution, we first examined the amount of radioactivity in the blood following injection. Blood levels of nanocarriers declined in a bi-phasic manner, with a distribution half-life ( $t_{1/2\alpha}$ ) of 2.9 h and an elimination half-life ( $t_{1/2\beta}$ ) of 34.9 h (Figure 4). Nearly a third of nanocarriers remained in circulation 24 h post-injection ( $31 \pm 2\%$  ID,  $18 \pm 2\%$  ID/g). These circulation time are consistent with circulation times for FNP nanocarriers measured by alternate techniques.<sup>53,54</sup> In contrast, previous studies of PEGylated radiolabeled nanocarriers produced by alternate techniques exhibit lower blood retention at 24 h (8-25% ID, 1-6% ID/g)<sup>29, 55-61</sup> and shorter circulation half-lives ( $t_{1/2\alpha}$ : 14 min-2.4 h,  $t_{1/2\beta}$ : 6-22.5 h)<sup>29,56,58,62</sup> (Supplementary Table 1). Our unique nanocarrier construct accounts for the longer circulation times. First, FNP imparts a dense PEG layer (2.25  $\text{nm}^2$  per chain for a 5k PEG),<sup>37</sup> effectively shielding the nanomaterial from opsonization. Second, we avoid the addition of surface charge to the nanocarriers, which inherently occurs for nanocarriers prepared by chelation, since for FNP the radiolabel is neutral and is in the core. Together, this likely delays a RES response that prematurely clears nanoprobe from the body.<sup>3,10-13</sup>

Based on the blood clearance half-lives, mice were euthanized at 5 min, 4 h, 10 h, 24 h, and 96 h post-injection and selected organs were harvested and weighed. The liver, spleen, kidney and thyroid were monitored to provide insight into *in vivo* particle stability over 96 hours. Decreasing radioactivity in the blood, heart, and lungs, and increasing radioactivity in the liver and spleen over time are consistent with gradual RES clearance for this size particle (Figure 5).<sup>9,63,64</sup> Although hepatic uptake dominates at 24 h post-injection ( $16 \pm 2\%$  ID/g),

previous studies of PEGylated  $^{64}\text{Cu}$ -labeled nanocarriers ranging from 20-30 nm demonstrated higher liver uptake at 24 h, ranging from 22 to 31% ID/g.<sup>31,54</sup>

Low kidney radioactivity (Figure 5) confirms that the nanocarriers tend to avoid renal clearance, partially accounting for the prolonged circulation time. Low lung and heart radioactivity (Figure 5) suggest that there is no specific binding of the nanocarriers despite the high blood perfusion level in these organ compartments.

At 24 h, the radioactivity in the thyroid is relatively low at  $0.11 \pm 0.09$  % ID, and at 96 h it only slightly increases to  $0.16 \pm 0.05$  % ID. Since free iodine naturally accumulates in the thyroid, low thyroid radioactivity over time indicates that minimal  $^{125}\text{I}$  leached from the radiolabeled nanocarrier core *in vivo*.<sup>65</sup> Thus, PEGylated [ $^{125}\text{I}$ ]PVPPh nanocarriers are circulating intact. For comparison, Novakova *et al.* injected the free polymer [ $^{125}\text{I}$ ] poly(D,L-lactide)-*block*-poly(ethylene oxide) into rats and found increasing uptake of radioactivity in the thyroid over 24 h.<sup>57</sup> In their study, radioiodine was covalently attached to poly(D,L-lactide) via an added *p*-methoxyphenol end group.<sup>57</sup> The high radioactivity in the thyroid 24 h post-injection ( $4 \pm 2$  % ID) was attributed to release of radioiodine from hydrolysis of the biodegradable poly(D,L-lactide) block.<sup>57</sup> Given that our particle components are non-biodegradable, free radioiodine would presumably result from dissociation and metabolism of the radiolabel covalently bound to the polyvinyl phenol in the core and would accumulate in the thyroid. However, thyroid radioactivity remains low over 96 hours particle stability *in vivo* over the evaluated time course.

The liver, spleen, kidney and thyroid were monitored to provide insight into *in vivo* particle stability over 96 hours. Examining the overall biodistribution: (1) the nanocarrier concentration in the liver and spleen increase as a function of time, (2) the radioactivity in the kidneys remains low, and (3) the radioactivity of the thyroid remains extremely low. Taken together, (1) and (2) indicate the particles are gradually cleared by the RES as expected for this size particle and the nanocarrier size appears to remain intact over 96 hours. Combined with the low thyroid radioactivity over 96 hours (3), the radiolabeled particles remain stable in circulation during evaluated time course.

The delayed RES clearance and relatively long circulation half-life *in vivo*, PEGylated [ $^{125}\text{I}$ ]PVPPh nanocarriers, are a promising platform for molecular imaging. Introducing a phenol chemical handle via encapsulation of PVPPh allows us to easily tag these materials with radioiodine to track their fate *in vivo* ultimately by non-invasive diagnostic means using PET or SPECT imaging.

#### 4. Conclusions

We produced PEGylated PVPPh nanocarriers via Flash NanoPrecipitation and successfully radiolabeled their phenol-containing core with  $^{125}\text{I}$  at high radiochemical yields (>90%). Radioiodination enabled facile characterization of *in vivo* nanocarrier fate and biodistribution. The nanocarriers demonstrated extended circulation half-lives ( $t_{1/2\beta} = 2.9$  h,  $t_{1/2\beta} = 34.9$  h) with 31% ID retained in the blood pool 24 h post-injection and gradual RES clearance (liver 17% ID (24 h), 19% ID (96 h); spleen 1.2% ID (24 h), 1.4% ID (96 h))



indicating the nanocarrier size appears to remain intact over 96 hours. Further, the very low thyroid radioactivity throughout the *in vivo* study indicate radiolabeled nanocarriers circulate intact over 96 hours. Given their delayed RES clearance and long circulation half-life *in vivo*, PEGylated [<sup>125</sup>I]PVPh nanocarriers are a promising platform for preclinical and translational imaging. This study provides a starting point for evaluation of the circulation and fate of nanoparticles produced by FNP based on size, charge, surface coating, and active targeting moieties. It leads directly to studies of targeting and biodistribution, which are extremely important as the field places more emphasis on targeted nanocarriers. The FNP process enables the preparation of targeted nanocarriers in a facile, and scalable manner.<sup>66,67</sup> Introducing a phenol chemical handle via encapsulation of PVPh allows us to easily tag these nanomaterials with radioiodine to track their fate *in vivo*, ultimately by noninvasive means using PET or SPECT imaging.

## Supplementary Material

Refer to Web version on PubMed Central for supplementary material.

## Acknowledgements

This work was supported by Princeton University's IP Accelerator Fund to RKP and Princeton University's Lidow Senior Thesis Fund to JNE. Additional support was provided by the Summer Undergraduate Program for Educating Radiation Scientists at the University of Pennsylvania (SUPERS@PENN) to AHH and NIH NCATS through grant KL2TR00139 to AMC. We would like to thank Dr. Istvan Pelczer for discussions regarding <sup>13</sup>C NMR.

## References

1. Psimadas D, Georgoulas P, Valotassiou V, Loudos G. J. Pharm. Sci. 2012; 7:2271–2280. [PubMed: 22488174]
2. Solon EG. Cell Tissue Res. 2015; 360:87–107. [PubMed: 25604842]
3. Branco de Barros AL, Tsourkas A, Saboury B, Cardoso V, Alavi A. EJNMMI Res. 2012; 2:39. [PubMed: 22809406]
4. Ting G, Chang CH, Wang HE. Anticancer Res. 2009; 29:4107–4118. [PubMed: 19846958]
5. Sun X, Huang X, Yan X, Wang Y, Guo J, Jacobson O, Liu D. ACS Nano. 2014; 8:8438–8446. [PubMed: 25019252]
6. Koehler L, Gagnon K, McQuarrie S, Wuest F. Molecules. 2010; 15:2686–2718. [PubMed: 20428073]
7. Chacko A-M, Divgi CR. Med. Chem. (Los. Angeles). 2011; 7:395–412.
8. Brechbiel M. Q J Nucl Med Mol Imaging. 2008; 52:166–173. [PubMed: 18043537]
9. Stockhofe K, Postema JM, Schieferstein H, Ross TL. Pharmaceuticals. 2014; 7:392–418. [PubMed: 24699244]
10. Arvizo RR, Miranda OR, Moyano DF, Walden C. a. Giri K, Bhattacharya R, Robertson JD, Rotello VM, Reid JM, Mukherjee P. PLoS One. 2011; 6:3–8.
11. Thiele L, Rothen-Rutishauser B, Jilek S, Wunderli-Allenspach H, Merkle HP, Walter E. J. Control. Release. 2001; 76:59–71. [PubMed: 11532313]
12. He C, Hu Y, Yin L, Tang C, Yin C. Biomaterials. 2010; 31:3657–3666. [PubMed: 20138662]
13. Howard MD, Jay M, Dziubla TD, Lu X. J. Biomed. Nanotechnol. 2008; 4:133–148.
14. Simone E, Zern BJ, Chacko A, Mikitsh JL, Muro S, V Stan R, Muzykantov VR. Biomaterials. 2012; 33:5406–5413. [PubMed: 22560201]
15. Cai W, Chen K, Li Z-B, Gambhir SS, Chen X. J. Nucl. Med. 2007; 48:1862–1870. [PubMed: 17942800]

16. Choi J, Park JC, Nah H, Woo S, Oh J, Kim KM, Cheon GJ, Chang Y, Yoo J, Cheon J. *Angew. Chem. Int. Ed. Engl.* 2008; 47:6259–6262. [PubMed: 18613191]
17. Gratton SEA, Pohlhaus PD, Lee J, Guo J, Cho MJ, DeSimone JM. *J. Control. Release.* 2007; 121:10–18. [PubMed: 17643544]
18. Sun Y, Yu M, Liang S, Zhang Y, Li C, Mou T, Yang W, Zhang X, Li B, Huang C, Li F. *Biomaterials.* 2011; 32:2999–3007. [PubMed: 21295345]
19. Chrastina A, Schnitzer JE. *Int. J. Nanomedicine.* 2010; 5:653–659. [PubMed: 20856841]
20. Lee CC, Yoshida M, Fréchet JMJ, Dy EE, Szoka FC. *Bioconjug. Chem.* 2005; 16:535–541. [PubMed: 15898719]
21. Shao X, Zhang H, Rajian JR, Chamberland DL, Sherman PS, Quesada CA, Koch AE, Kotov NA, Wang X. *ACS Nano.* 2011; 5:8967–8973. [PubMed: 22003968]
22. Park JC, Yu MK, Il An G, Il Park S, Oh J, Kim HJ, Kim JH, Wang EK, Hong IH, Ha YS, Choi TH, Jeong KS, Chang Y, Welch MJ, Jon S, Yoo J. *Small.* 2010; 6:2863–2868. [PubMed: 21104828]
23. Ballot S, Noiret N, Hindré F, Denizot B, Garin E, Rajerison H, Benoit JP. *Eur. J. Nucl. Med. Mol. Imaging.* 2006; 33:602–607. [PubMed: 16450136]
24. Kennel SJ, Woodward JD, Rondinone AJ, Wall J, Huang Y, Mirzadeh S. *Nucl. Med. Biol.* 2008; 35:501–514. [PubMed: 18482688]
25. McDevitt MR, Chattopadhyay D, Jaggi JS, Finn RD, Zanzonico PB, Villa C, Rey D, Mendenhall J, Batt CA, Njardarson JT, Scheinberg DA. *PLoS One.* 2007; 2:907.
26. Rossin R, Muro S, Welch MJ, Muzykantov VR, Schuster DP. *J. Nucl. Med.* 2008; 49:103–111. [PubMed: 18077519]
27. Akizawa H, Uehara T, Arano Y. *Adv. Drug Deliv. Rev.* 2008; 60:1319–1328. [PubMed: 18508156]
28. Haubner R, Wester H-J. *Curr. Pharm. Des.* 2004; 10:1439–1455. [PubMed: 15134568]
29. Zhou M, Zhang R, Huang M, Lu W, Song S, Melancon MP, Tian M, Liang D, Li C. *J. Am. Chem. Soc.* 2010; 132:15351–15358. [PubMed: 20942456]
30. Vonarbourg A, Passirani C, Saulnier P, Benoit JP. *Biomaterials.* 2006; 27:4356–4373. [PubMed: 16650890]
31. Gref R, Domb A, Quellec P, Blunk T, M. R.H. Verbavatz JM, Langer R. *Adv. Drug Deliv. Rev.* 1995; 16:215–233. [PubMed: 25170183]
32. Budijono SJ, Russ B, Saad W, Adamson DH, Prud'homme RK. *Colloids Surf., A.* 2010; 360:105–110.
33. Shen H, Hong S, Prud'Homme RK, Liu Y. *J. Nanoparticle Res.* 2011; 13:4109–4120.
34. D'Addio SM, Prud'homme RK. *Adv. Drug Deliv. Rev.* 2011; 63:417–426. [PubMed: 21565233]
35. A Petros R, DeSimone JM. *Nat. Rev. Drug Discov.* 2010; 9:615–627. [PubMed: 20616808]
36. Jing Han CWM, Zhu Zhengxi, Qian Haitao, Wohl Adam R, Beaman Charles J, Hoye Thomas R. *J. Pharm. Sci.* 2012; 101:4018–4023. [PubMed: 22777753]
37. D'Addio SM, Saad W, Ansell SM, Squiers JJ, Adamson D, Herrero-Alonso M, Wohl AR, Hoye TR, Macosko CW, Meyer LD, Vauthier C, Prud'homme RK. *J. Control Release.* 2012; 162:208–217. [PubMed: 22732478]
38. Edgar KJ, Falling SN. *J. Org. Chem.* 1990; 55:5287–5291.
39. Zern BJ, Chacko AM, Liu J, Greineder CF, Blankemeyer ER, Radhakrishnan R, Muzykantov V. *ACS Nano.* 2013; 7:2461–2469. [PubMed: 23383962]
40. Nishiyama N, Kataoka K. *Pharmacol. Ther.* 2006; 112:630–648. [PubMed: 16815554]
41. Koo OM, Rubinstein I, Onyuksel H. *Nanomedicine Nanotechnology, Biol. Med.* 2005; 1:193–212.
42. Yokoyama M. *J. Exp. Clin. Med.* 2011; 3:151–158.
43. Duan X, Li Y. *Small.* 2013; 9:1521–1532. [PubMed: 23019091]
44. Decuzzi P, Godin B, Tanaka T, Lee SY, Chiappini C, Liu X, Ferrari M. *J. Control. Release.* 2010; 141:320–327. [PubMed: 19874859]
45. Figueroa CE, Reider P, Burckel P, Pinkerton AA, Prud'homme RK. *Ther. Deliv.* 2012; 3:1269–79. [PubMed: 23259248]
46. Alexander NM. *J. Biol. Chem.* 1974; 249:1946–1952. [PubMed: 4817970]
47. Tadashi Kometani TJ, Watt David S. *Tetrahedron Lett.* 1985; 26:2043–2046.

48. Smith WB, Proulx TW, Worth F. *Org. Magn. Reson.* 1976; 8:205–207.
49. Chacko AM, Qu W, Kung HF. *J. Med. Chem.* 2008; 51:5690–5701. [PubMed: 18800764]
50. Bolton AE, Hunter WM. *Biochem. J.* 1973; 133:529–539. [PubMed: 4733239]
51. Sun G, Xu J, Hagooley A, Rossin R, Li Z, Moore DA, Hawker CJ, Welch MJ, Wooley KL. *Adv. Mater.* 2007; 19:3157–3162.
52. Jagoda EM, Vaquero JJ, Seidel J, Green MV, Eckelman WC. *Nucl. Med. Biol.* 2004; 31:771–779. [PubMed: 15246368]
53. Ansell SM, Johnstone SA, Tardi PG, Lo L, Xie S, Shu Y, Harasym TO, Harasym NL, Williams L, Bermudes D, Liboiron BD, Saad W, Prud'homme RK, Mayer LD. *J. Med. Chem.* 2008; 51:3288–3296. [PubMed: 18465845]
54. Pinkerton NM, Gindy ME, Calero-DdelC VL, Wolfson T, Pagels RF, Adler D, Gao D, Li S, Wang R, Zevon M, Yao N, Pacheco C, Therien MJ, Rinaldi C, Sinko PJ, Prud'homme RK. *Adv. Healthcare Mater.* 2015; 4:1376–1385.
55. Rossin R, Pan D, Qi K, Turner JL, Sun X, Wooley KL, Welch MJ. *J. Nucl. Med.* 2005; 46:1210–1219. [PubMed: 16000291]
56. Glaus C, Rossin R, Welch MJ, Bao G. *Bioconjugate Chem.* 2010; 21:715–722.
57. Novakova K, Laznicek M, Rypacek F, Machova L. *J. Bioact. Compat. Polym.* 2002; 17:285–296.
58. Yamamoto Y, Nagasaki Y, Kato Y, Sugiyama Y. *J. Control. Release.* 2001; 77:27–38. [PubMed: 11689257]
59. Zhao Y, Sultan D, Detering L, Cho S, Sun G, Pierce R, Wooley KL, Liu Y. *Angew. Chemie - Int. Ed.* 2014; 53:156–159.
60. Melancon MP, Lu W, Yang Z, Zhang R, Cheng Z, Elliot AM, Stafford J, Olson T, Zhang JZ, Li C. *Mol. Cancer Ther.* 2008; 7:1730–1739. [PubMed: 18566244]
61. Wang Y, Liu Y, Luehmann H, Xia X, Brown P, Jarreau C, Welch M, Xia Y. *ACS Nano.* 2012; 6:5880–5888. [PubMed: 22690722]
62. Zhang G, Yang Z, Lu W, Zhang R, Huang Q, Tian M, Li L, Liang D, Li C. *Biomaterials.* 2009; 30:1928–1936. [PubMed: 19131103]
63. Peracchia MT, Fattal E, Desmaële D, Besnard M, Noël JP, Gomis JM, Appel M, D'Angelo J, Couvreur P. *J. Control. Release.* 1999; 60:121–128. [PubMed: 10370176]
64. Bazile D, Prud'Homme C, Bassoullet MT, Marlard M, Spenlehauer G, Veillard M. *J. Pharm. Sci.* 1995; 84:493–498. [PubMed: 7629743]
65. Adam MJ, Wilbur DS. *Chem. Soc. Rev.* 2005; 34:153–163. [PubMed: 15672179]
66. Akbulut M, Ginart P, Gindy ME, Theriault C, Chin KH, Soboyejo W, Prud'homme RK. *Adv. Funct. Mater.* 2009; 19:718–725.
67. D'Addio SM, Baldassano S, Shi L, Cheung L, Adamson DH, Bruzek M, Anthony JE, Laskin DL, Sinko PJ, Prud'homme RK. *J. Control. Release.* 2013; 168:41–49. [PubMed: 23419950]

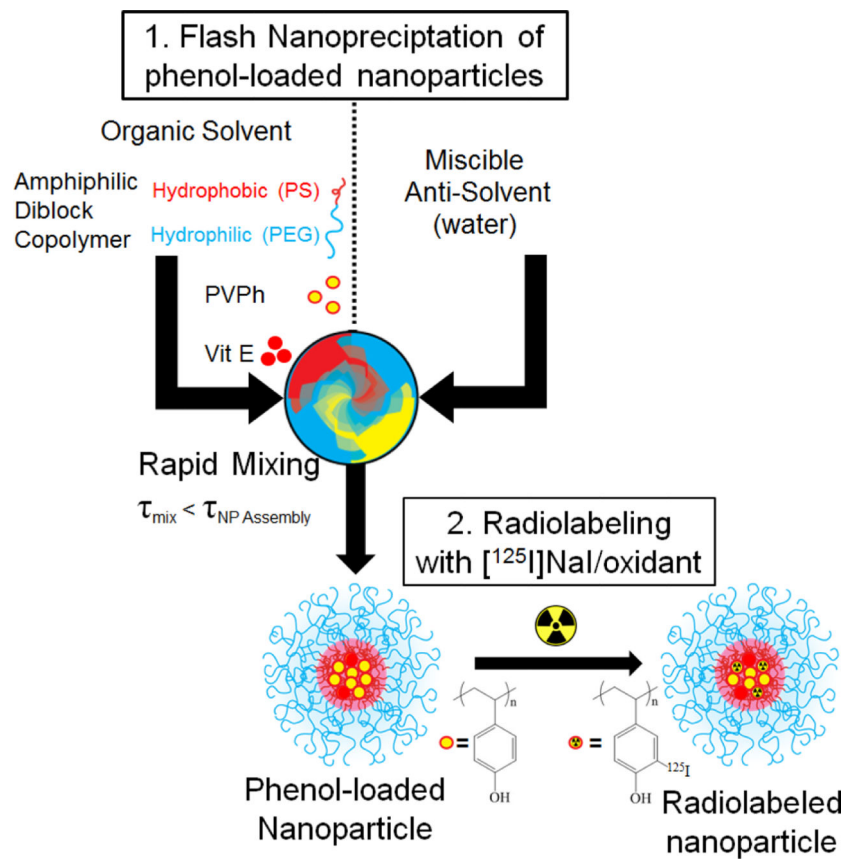


**Figure 1.** Schematic of nanocarrier synthesis by FNP and subsequent radiolabeling of the PVPh core with  $^{125}\text{I}$ .

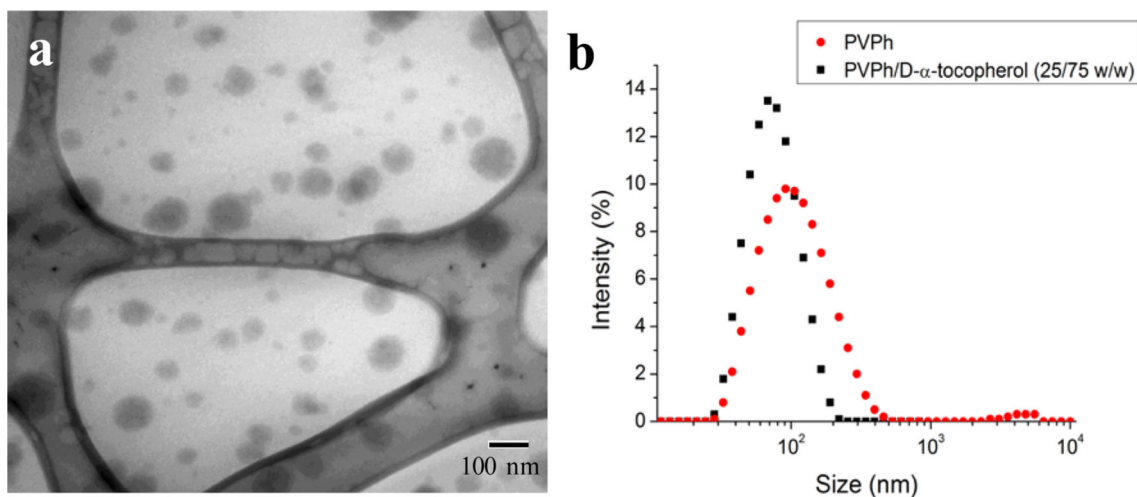


**Figure 2. Characterization of PEGylated PVPh nanocarriers synthesized using FNP**

a) Representative TEM micrograph of nanocarriers. Nanocarriers appear smaller than the hydrodynamic radius measured with DLS because the PEG layer is not sufficiently electron dense to be visible with TEM.

b) Size distribution of nanocarriers with ( $79 \pm 3$  nm, PDI  $0.151 \pm 0.009$ ) and without ( $120 \pm 8$  nm, PDI  $0.228 \pm 0.008$ ) D- $\alpha$ -tocopherol. Coprecipitation of PVPh and D- $\alpha$ -tocopherol reduced resulting nanocarrier size.

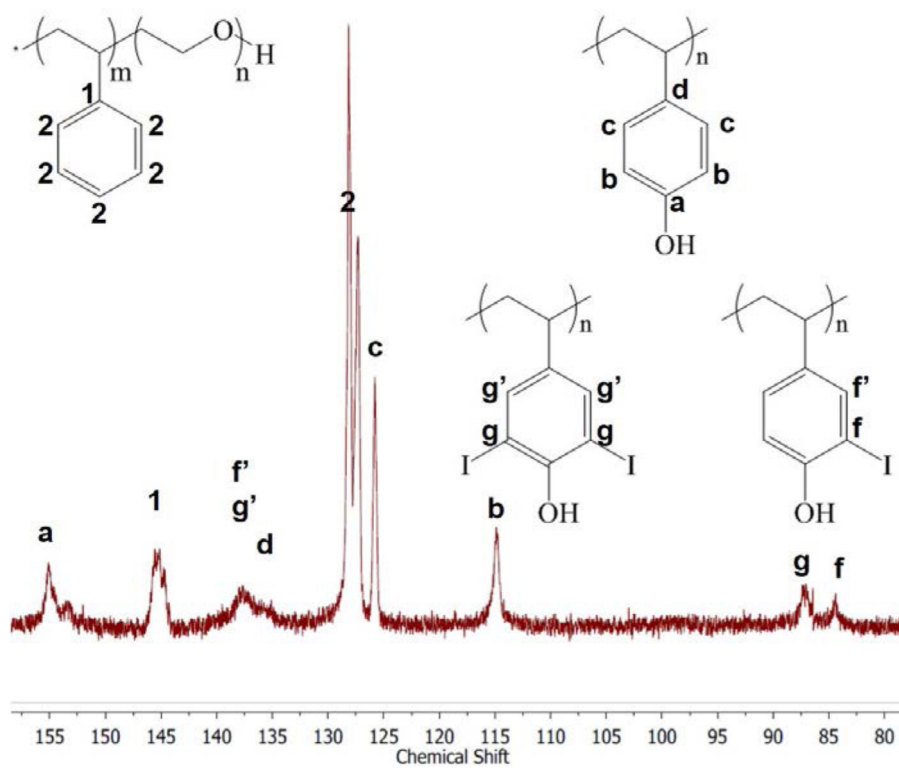


**Figure 3.** Aromatic section of  $^{13}\text{C}$ -NMR spectrum of nanocarrier components redissolved in deuterated DMSO following iodination reaction and purification. Iodination causes an upfield shift of the carbon *ortho* to phenol from 115 to 84 ppm. Di-iodination of polyvinyl phenol core is evident from the downfield shift of the iodinated peak to 87 ppm.

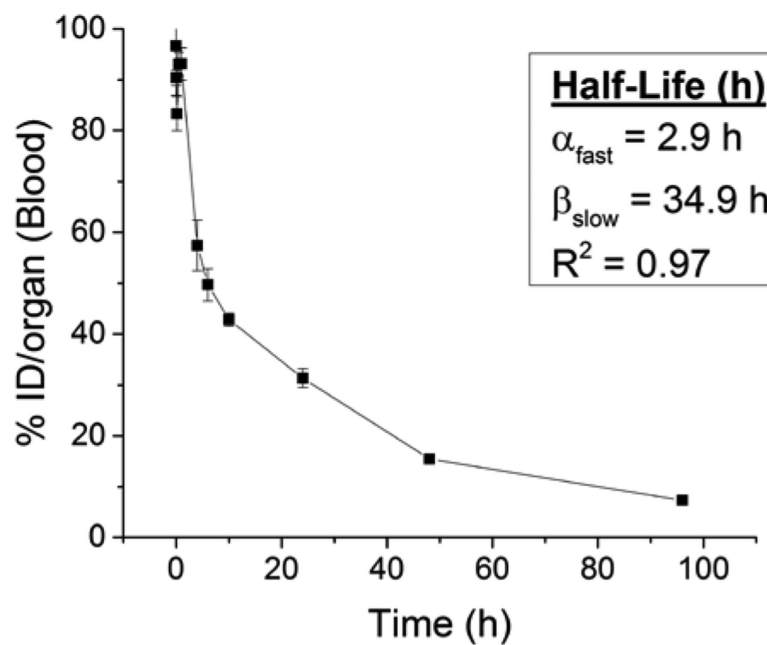


**Figure 4.** Blood clearance profile of radiolabeled nanocarriers following intravenous injection in healthy mice (n = 3 per time point).

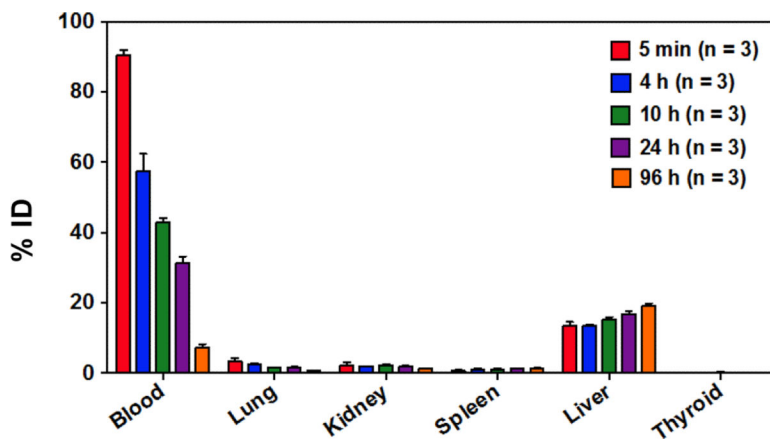


**Figure 5.** Biodistribution of radiolabeled nanocarriers in the blood, lung, kidney, spleen, liver, thyroid, and brain over time reported as % ID (n=3). Decreasing radioactivity in the blood and increasing radioactivity in the liver and spleen over time is consistent with gradual RES clearance of nanocarriers and prolonged systemic circulation. Decreasing radioactivity in the kidney suggests minimal renal clearance. Low lung radioactivity suggests that there is no specific binding despite the high blood perfusion level. Low thyroid radioactivity suggests that  $^{125}\text{I}$  did not leach from nanocarrier core.